Identification of karst features using seismic P-wave tomography and resistivity anisotropy measurements

Abdullah Karaman · Turhan Karadayılar

Abstract A football stadium with a capacity of a hundred thousand spectators is under construction over a karst terrain, 10 km west of the old town of Istanbul, Turkey. A large cavity of approximately 30 m^3 was detected beneath the sports field through a number of boreholes so that a geophysical survey was required to further investigate a portion of the sports field. We utilized seismic refraction tomography and dc-electrical method with rotated Wenner array to delineate zones with solution voids and cavities. Total core recovery (TCR) was 5–15% from boreholes where zones with low velocities were identified through tomographic inversion, whereas TCR values were above 60% in zones with higher velocities. Both low velocity zones in the tomographic images and increasing resistivity anisotropy with depth appear to indicate that the cavity extends toward the west and south at a depth of approximately 8 m, although the southward and westward extension changes in character.

Keywords Karst · Cavity detection · Seismic tomography · Resistivity anisotropy · Geohazard

Received: 17 July 2003 / Accepted: 24 November 2003
Published online: 21 January 2004

A. Karaman (✉)
Department of Geophysics,
Istanbul Technical University,
80626 Maslak Istanbul, Turkey
E-mail: karaman@itu.edu.tr

A. Karaman
EMA Geophysics, Bağdat Cad.,
No:136/8 Maltepe, Istanbul, Turkey

T. Karadayılar
ZETAŞ, Silahtarbahçe Sok.
Soyak Sitesi Selamiali Mah.,
B7/1, 81150 Üsküdar Istanbul, Turkey
E-mail: karadayilart@zetas.com.tr

Introduction

The city of Istanbul, Turkey, is being rigorously prepared to host one of the upcoming Olympic Games. For this purpose, an Olympic-size football stadium with a capacity of a hundred thousand spectators is under construction over a karst terrain, 10 km west of the old town of Istanbul. Geohazards have been carefully considered for the tribunes, and every indication of a large cavity has been carefully examined through the drilling of a number of boreholes. Structural load has been distributed over a very large area through using wide foundation footings to avoid damage that may be inflicted to the structure due to a cover-collapse. The sports field, on the other hand, was investigated by about 25 boreholes leading to the detection of a large cavity of approximately 30 m^3. However, those that might have remained unidentified as conceptually illustrated in Fig. 1 created serious concern. The borehole A in Fig. 1 crosses a small portion of the void while B advances in the solid rock only. Therefore, a geophysical survey was required to further investigate the endangered portion of the sports field.

Dissolution of soluble rocks such as limestone and dolomites by groundwater causes karst to develop, characterized by solution voids and cavities, sinkholes, sinking streams and presence of irregular rock surfaces with soil-filled slots and pinnacles (Carpenter and others 1998). Such a situation is a challenge for foundation engineering and construction work because of the changing nature of the soil and rock that support the structures (Knott and others 1993). Undetected voids are the most hazardous among these karst features because they can lead to a collapse of the structures built above (Mylroie and Carew 1997). So-called cover-collapse that produces a geohazard may be triggered by the disturbances of various origins, for example, changes in the hydraulic regime, loading events of rather short duration or moderate magnitude, dynamic loading, blasting and even a small earthquake (Tharp 1997). The passage of heavy and vibrating construction equipment may also trigger a cover-collapse. The detection of such weak zones, therefore, is extremely important to mitigate geohazards during both construction operations and the lifetime of the building.

Cavity detection and delineation in a karst terrain has received increased attention in recent studies. Paukstys and others (1997) develop guidelines and environmentally

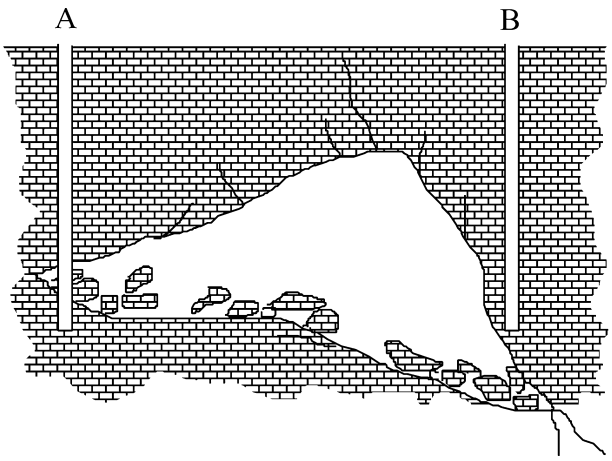

Fig. 1
Conceptual illustration of a cavity that may be missed by borehole drilling when their spatial distribution of the boreholes is insufficient

friendly measures to mitigate geological hazards. Benson and Yuhr (1993) summarized the common geophysical methods that may be utilized for cavity detection and mapping, and conceptually discussed their spatial sampling capabilities and limitations. Kaufmann and Quinif (1997) utilized dc-electrical methods and discussed the utility of geohazard maps for regional development planning. In a more comprehensive work, Carpenter and others (1998) utilized electromagnetic methods including ground penetrating radar (GPR), and dc-electrical resistivity methods to characterize buried sinkholes in a karst terrain. There are several other studies that applied dc-electrical resistivity methods with various electrode configurations (e.g., Lambert 1997; Gautam and others 2000; Guerin and Benderitter 1995). McDowell and Hope (1993) used cross-hole and surface-to-borehole scanning procedures for P-wave tomography. Unlike these previous studies, we used seismic refraction tomography as described in Karaman and Carpenter (1997) and dc-electrical methods with rotated Wenner array as described in Carpenter and others (1991) to delineate zones with solution voids and cavities beneath the sports field. The choice of methods and our approach for the geophysical measurements were mostly driven by the limited dimensions of the field.

Fig. 2
Map of the elliptical sports field showing the previously detected cavity, extension of tomographic arrays (*shaded polygons*), location of the boreholes, and sites of the azimuthal resistivity measurements (marked by *W#*)

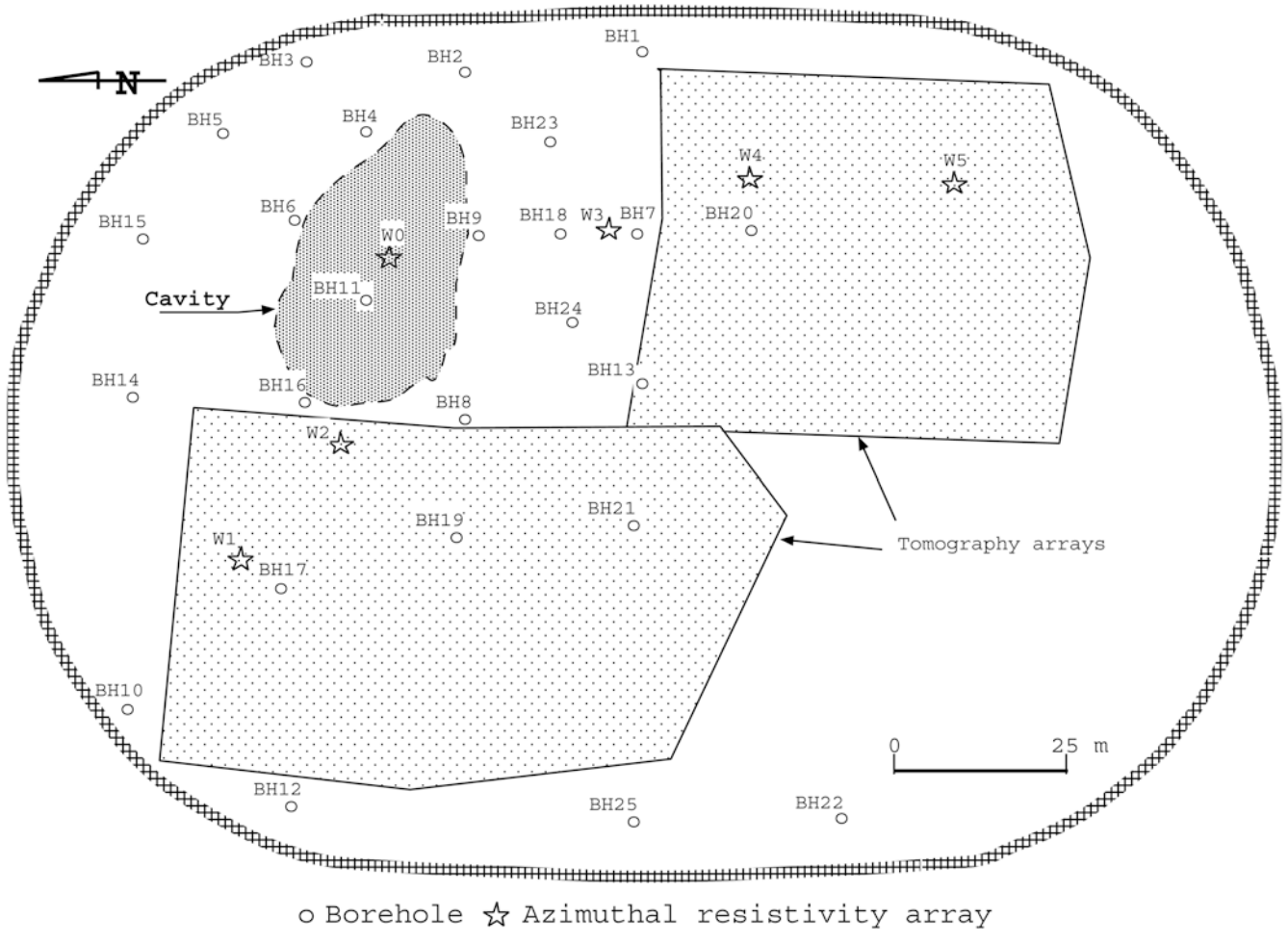

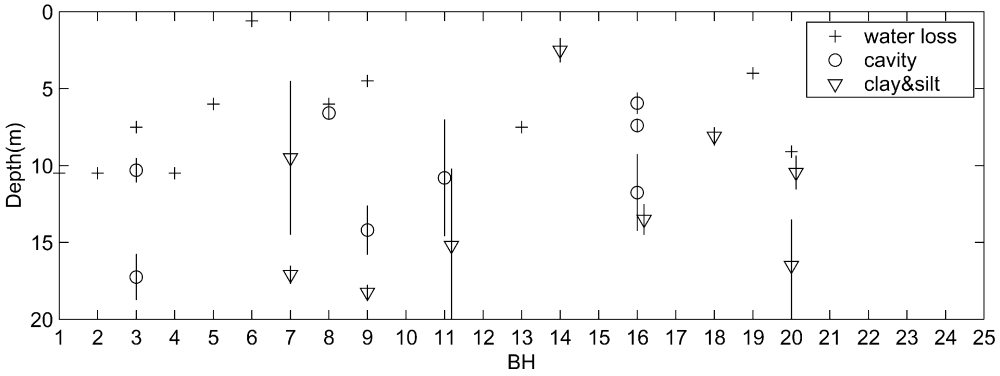

Fig. 3
Summary of findings of 25 boreholes. The *horizontal axis* shows the borehole numbers as labeled in Fig. 2. The *vertical bars* show the depth intervals of features (water loss, cavity or clay and silt) that were encountered during the drilling

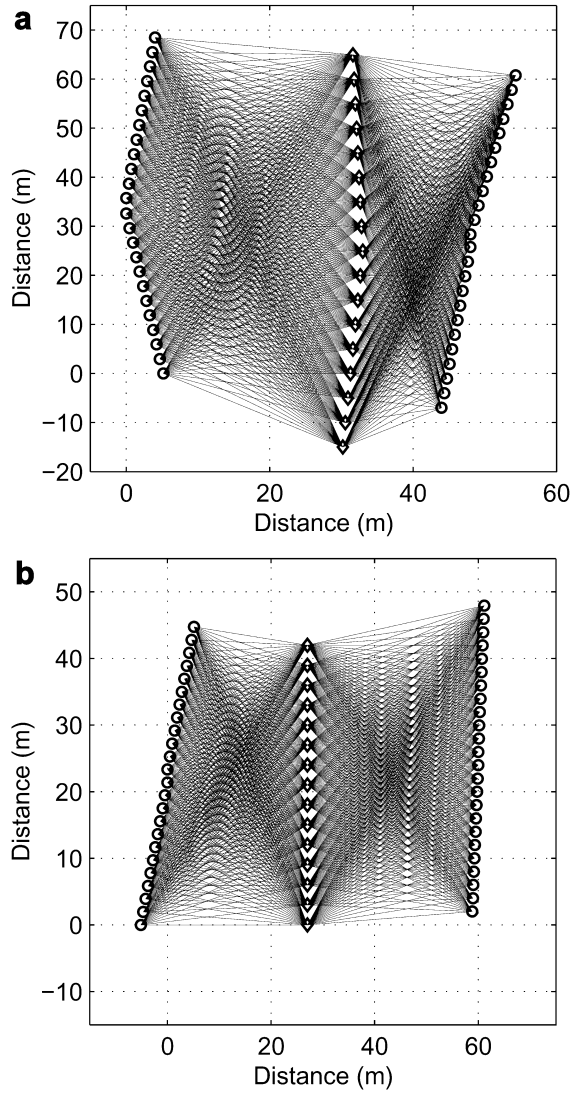

Fig. 4
A plan view of the source and receiver locations for the tomography survey, together with some of the raypaths. These tomographic arrays cover the west (**a**) and the south (**b**) of the previously detected cavity

Site description

The location of the study site is about 10 km west of the old town of Istanbul, Turkey, where 80–100-m-thick limestone bedrock occasionally underlies a thin topsoil that forms a gently rolling topography. The bedrock limestone at the construction site exhibits occasional karst features such as cavities and soil-filled solution voids, but preserves its solid rock structure. During the geophysical measurements, the tribunes on four sides of the sports field were under construction. The topsoil and a few tens of centimeters of limestone bedrock within the field were removed for preparation of a perfectly flat ground surface. Therefore, our measurements required no correction due to topography. The groundwater level at the time of the survey was at a depth of 50 m from the ground surface and practically had no effect on the measurements. Figure 2 illustrates the location of the previously detected cavity of volume approximately 30 m^3 within the elliptical sports field. About 25 boreholes were drilled, the findings of which are graphically illustrated in Fig. 3. The depths at which circulation water losses started indicate the presence of solution voids. The depth intervals at which a cavity or clay and silt were detected while drilling are also displayed.

Seismic data acquisition and analysis

We acquired digital seismic data using two 12-channel EG&G SmartSeis exploration seismographs (total 24 channels). The P-wave energy source was a 6-kg sledgehammer vertically striking a metal plate. The receivers were 40-Hz Mark vertical geophones. A sampling interval of 0.05 ms was used; energy from repeated sledgehammer blows was stacked to improve the signal-to-noise (S/N) ratio.
Two target locations for the tomographic experiments in the sports field are illustrated in Fig. 2. The source-receiver geometry and ray-paths for the two tomographic experiments are plotted in Fig. 4. Geophones were placed every 3 m along the east and west edges of the arrays. Source points in these experiments were placed every 5 m along a line in the center of the arrays. A total of 48 receivers were spread along the east and west edges of the arrays, recording signals from 17 sources. Most of the geophones were grouted to the ground with plaster to provide the ground coupling. The data acquisition geometry and the data analysis for the refraction tomography used in this study are the same as presented in Karaman

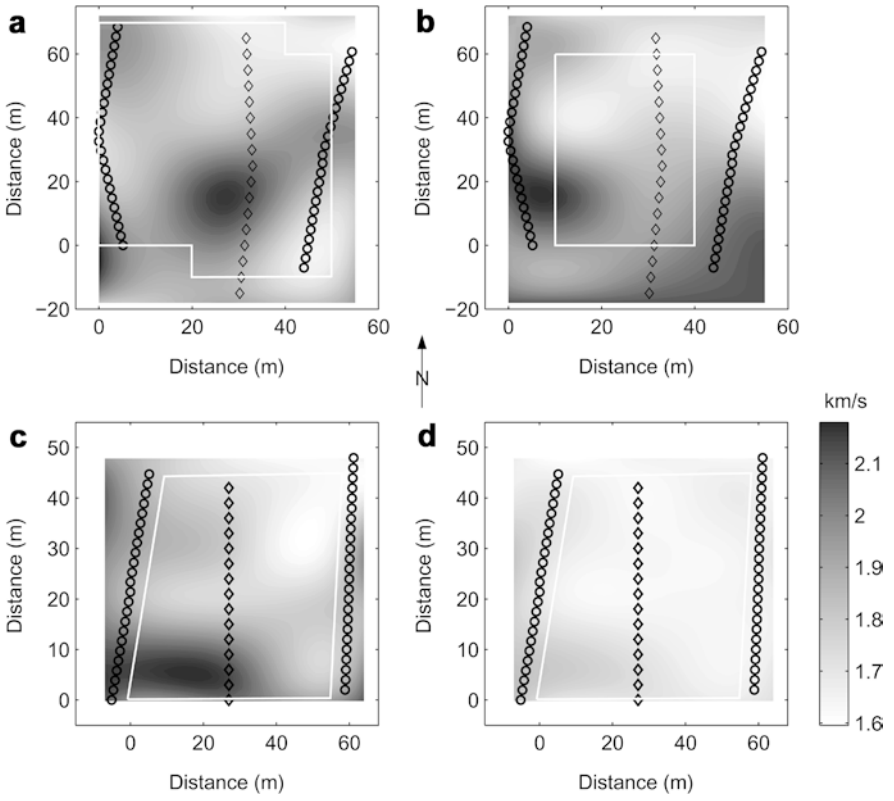

Fig. 5
P-wave velocity images of the horizontal slices that represent the 8-m-thick top layer (**a** and **c**) and underlying half-space (**b** and **d**). The shot and receiver locations are *diamonds* and *circles*, respectively. *White polygons* denote the areas where a reliable solution was obtained after tomographic inversion

and Carpenter (1997). The tomographic models were constructed by dividing each volume of interest into $10 \times 10 \times 2$ cells along x, y, and z (the depth) directions. The images representing horizontal P-wave velocity slices calculated after four iterations are illustrated in Fig. 5. Figure 5a, c represent the average velocity distributions for the top layer with a thickness of 8 m. The velocity distributions for the half-space beneath the top layer are given in Fig. 5b, d. Cells that were reliably resolved in these images are roughly bounded by the polygons with a solid white line.

Azimuthal resistivity measurements

The five pivot points of the electrodes for the azimuthal resistivity measurements are marked in Fig. 2. At each location a Wenner electrode array was rotated incrementally by 30° up to 180°, about the center of the array, and the resistivity value was calculated at each increment by using the measured potential between the potential electrodes. The measurements were carried out for exploration depths (three times the electrode spacing) of 2, 4, 8, and 12 m to obtain four resistivity anisotropy ellipses. Table 1 lists the azimuth values of the major axes (θ) and the percent resistivity anisotropy values calculated using $\alpha = (1-a/b) \times 100$ where a and b are the lengths of the minor and major axes. An example resistivity ellipse measured for the depth of 12 m at W3 is illustrated in Fig. 6.

Results and discussions

The images presented in Fig. 5 exhibit a non-uniform velocity distribution with small velocity contrast. The boreholes within and near the tomographic arrays (BH7, 8, 11, 13, 16, 17, 19, 20 and 21) had TCR (total core recovery) of 5–15% in low velocity zones whereas TCR was comparatively high (e.g. above 60%) in the zones with higher velocities. However, neither of these boreholes except

Table 1
The percent anisotropy (α) and the azimuth values of the major axes (θ, in degrees) with depths

		W0		W1		W2		W3		W4		W5	
		z	θ	z	θ	Z	θ	z	θ	z	θ	z	θ
Depth (meters)	2	26	150	13	30	11	60	8	30	18	30	20	150
	4	26	30	24	30	18	160	41	60	70	0	17	30
	8	46	30	49	150	30	90	17	170	23	60	55	90
	12	53	27	33	90	38	90	58	75	40	150	44	–

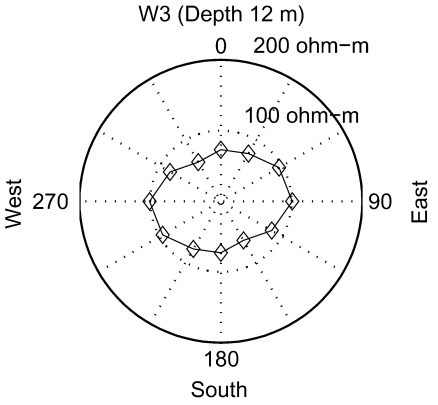

Fig. 6
An azimuthal resistivity variation curve that is used to calculate the resistivity anisotropy. The major axis of this *ellipse* describes the direction along which the electrical current experiences the highest resistance

BH11 and BH16 encountered a cavity of significant size. Azimuthal resistivity measurements, on the other hand, indicated increasing anisotropy with depth, although the azimuths of the resistivity ellipses seem to be inconsistent. This may be because of the change in the geometry and the size of the anomalous zone. The low velocity zones in the velocity images and increasing resistivity anisotropy with depth may indicate that the existing cavity extends toward the west and south at a depth of approximately 8 m (this is the resolution obtained from the inversion procedure). However, extensive clay presence at BH7 and BH20 (Fig. 3) suggests a clay- and silt-filled cavity that would also produce lower velocity values than for limestone. The character of the westward extension seems to be complicated since it is difficult to attribute the low velocity directly to the presence of a large cavity. This uncertainty was clarified through an additional seismic experiment: the seismic source was kept right above the previously detected cavity near BH11 and the receivers were kept on a line toward north-south and east-west directions. All of the seismic records that were acquired through this experiment appeared to be extremely ringy, i.e., a wave train with large amplitudes lasting until the end of the seismic records was observed. This phenomenon was not observed elsewhere. Therefore, we assume the westward extension is a zone of solution voids of insignificant size.

Conclusions

With this study we investigated a portion of the sports field to identify a possible cavity that may pose a hazard to the ongoing construction operations. Seismic refraction tomography along with resistivity anisotropy measurements appear to yield satisfactory results to delineate zones of cavities and clay- and silt-filled cavities. However, the sensitivity of the seismic measurements for the purpose of tomographic imaging has to be taken into consideration and seismic tomography needs to be used with extra caution. For example, the sampling interval is suggested to be kept on the order of a few nanoseconds for accurate travel time readings. The starting model for the tomographic inversion has to be carefully tested since the final velocity field will partially depend on the initial model. Azimuthal resistivity measurements appear to provide very useful information and are suitable when the field is limited in size.

Acknowledgments This project was carried out for the main contractor Istanbul Stadium Builders J.V. The complete geotechnical work was carried out by Zemin Teknolojisi A.Ş. (ZETAŞ) under the directorate of Turan Durgunoğlu who has requested the implementation of this project. We would like to thank Kadem Ekşi for providing the resources of EMA Geophysics for the measurements. As time was scarce because the entire construction operations were to be ceased for the geophysical measurements, Mehmet Abidin, Mehmet Baş, Mehmet Kocaman, Mehmet Güler, Nevzat Mengüllüoğlu, Selçuk Karaman, Burak A. Tunalı, and Şakir Şahin, all from EMA Geophysics, worked diligently for a day and a night to ensure the top quality seismic and resistivity data. We also would like to thank to the site engineers of ZETAŞ, especially Serdar Elgun, for carefully supervising the drillings and for providing us with reliable borehole data, and Gülçin Tezel for her field assistance. The principle author is a consulting geophysicist for EMA Geophysics through an agreement 01-03-001 with ITU.

References

Benson RC, Yuhr L (1993) Spatial sampling considerations and their applications to characterizing fractured rock and karst systems. In: Beck BF (ed) Applied karst geology. AA Balkema, Rotterdam, pp 99–113

Carpenter PJ, Calkin SF, Kaufmann RS (1991) Assessing a fractured landfill cover using electrical resistivity and seismic refraction techniques. Geophysics 56(11):1896–1904

Carpenter PJ, Doll WE, Kaufmann RD (1998) Geophysical character of buried sinkholes on the Oak Ridge Reservation, Tennessee. J Environ Eng Geophys 3:133–145

Gautam P, Pant SR, Ando H (2000) Mapping of subsurface karst structure with gamma ray and electrical resistivity profiles: a case study from Pokhara Valley, central Nepal. J Appl Geophys 45:97–110

Guerin R, Benderitter Y (1995) Shallow karst exploration using MT-VLF and DC resistivity methods. Geophys Prospect 43:635–653

Karaman A, Carpenter PJ (1997) Fracture density estimates in glaciogenic deposits from P-wave velocity reductions. Geophys 62(1):138–148

Kaufmann O, Quinif Y (1997) Cover collapse sinkholes in the "Tournaisis" area, southern Belgium. In: Beck BF, Stephenson JB, Herring JG (eds) The engineering geology and hydrogeology of karst terranes. AA Balkema, Rotterdam, pp 41–47

Kesseru Z (1997) Assessing the risk of cave-collapse sinkholes using analogous information from mining. In: Beck BF, Stephenson JB, Herring JG (eds) The engineering geology and hydrogeology of karst terranes. AA Balkema, Rotterdam, pp 55–60

Knott DL, Newman FB, Gonzalez LFR, Gray RE (1993) Foundation engineering practice for bridges in karst areas. In: Beck BF (ed) Applied karst geology. AA Balkema, Rotterdam, pp 224–230

Lambert DW (1997) Dipole–dipole D.C. resistivity surveying for exploration of karst features. In: Beck BF, Stephenson JB, Herring JG (eds) The engineering geology and hydrogeology of karst terranes. AA Balkema, Rotterdam, pp 413–418

McDowell P, Hope V (1993) The location and delineation of karst and solution collapse features by acoustic tomography. In: Beck BF (ed) Applied karst geology. AA Balkema, Rotterdam, pp 123–129

Mylroie JE, Carew JL (1997) Land use and carbonate island karst. In: Beck BF, Stephenson JB, Herring JG (eds) The engineering geology and hydrogeology of karst terranes. AA Balkema, Rotterdam, pp 3–12

Paukstys B, Cooper AH, Arustiene J (1997) Planning for gypsum geohazards in Lithuania and England. In: Beck BF, Stephenson JB, Herring JG (eds) The engineering geology and hydrogeology of karst terranes. AA Balkema, Rotterdam, pp 3–12

Tharp TM (1997) Mechanics of formation of cover-collapse sinkholes. In: Beck BF, Stephenson JB, Herring JG (eds) The engineering geology and hydrogeology of karst terranes. AA Balkema, Rotterdam, pp 29–36

Yaoru L, Cooper AH (1997) Gypsum karst geohazards in China. In: Beck BF, Stephenson JB, Herring JG (eds) The engineering geology and hydrogeology of karst terranes. AA Balkema, Rotterdam, pp 117–126